JMEPEG (2018) 27:5427–5437
https://doi.org/10.1007/s11665-018-3626-x

1059-9495/$19.00

Sliding Wear Behavior of an AISI 440B Martensitic Stainless Steel Lubricated with Biodiesel and Diesel–Biodiesel Blends

Arlei Franz Venske, Victor Velho de Castro, Eleani Maria da Costa, and Carlos Alexandre dos Santos

(Submitted October 26, 2017; in revised form July 16, 2018; published online September 13, 2018)

The aim of this work was to analyze the effect of biodiesel and diesel–biodiesel blends on the sliding wear behavior of AISI 440B martensitic stainless steel. Lubricated tests were performed on AISI 440B martensitic stainless steel samples using Brazilian commercial diesel (containing 7 vol.% biodiesel), pure biodiesel, and diesel–biodiesel blends with biodiesel additions of 20% v/v, 30% v/v, and 50% v/v. Non-lubricated tests were also performed. The stainless steel was analyzed in the as-received condition (annealed) and after heat treatments (quenched and tempered at different temperatures), using a pin-on-disk device with an alumina pin, at a 1.8 m/s sliding speed, 14.7 N load, and 4400 m sliding distance, following the ASTM G99-04 Standard. Wear track widths, wear coefficients, and wear track surfaces were analyzed by optical and scanning electron microscopy. The results showed that AISI 440B presented the worst wear behavior in the dry condition with a microstructure characterized by a ferritic matrix and dispersed carbides (annealed condition). The wear resistance increased with the increase in biodiesel content due to the matrix strengthening by the martensitic transformation (heat-treated condition). When the biodiesel content was superior to 50% v/v, a reverse result was found. The observed wear mechanism was abrasive in all conditions. A − 1.35 power law coefficient characterized the wear coefficient as a function of biodiesel content for the annealed condition and a − 0.95 power law coefficient for the heat-treated conditions.

Keywords biodiesel, heat treatment, microstructures, pin on disk, stainless steel, wear

1. Introduction

Use of biodiesel as a substitute for fossil diesel has intensified in recent years, and countries in the European Union, Asia, North America, and South America now have public policies to increase the percentage of biodiesel added to petroleum diesel. In this context, Brazil holds an important position when compared to other countries. Today, Brazilian commercial diesel contains 7% biodiesel, which is expected to reach 10% by 2020 (Ref 1).

Due to the environmental preoccupation related to global climate change, and the necessity to reduce greenhouse gas emissions, mainly sulfur oxides, fossil diesel now has a low sulfur concentration, the consequence of which is lower fuel lubricity and a higher potential for increased wear of metallic parts under friction. When biodiesel is added to diesel, the lubricity increases, and consequently, the wear may decrease (Ref 2, 3).

Although there are numerous studies on biodiesel lubricity and its physical and chemical properties, there is a lack of information on the metallurgical interaction of biodiesel with metallic materials such as carbon steels, stainless steels, and non-ferrous alloys, especially on their wear characteristics in conventional diesel engines. Many studies have reported the effect of biodiesel addition on the lubricity of diesel–biodiesel blends. Aspects such as temperature, feedstocks, and friction conditions have also been analyzed to understand the lubrication properties and material interactions with biofuel. Lubricity decreases when temperature increases, and consequently, both friction and wear increase, as shown by Hasseb et al. (Ref 4) using palm biodiesel, four-ball wear tests, and temperatures range of 30-75 °C. When the temperature was fixed at 75 °C and the speed was increased from 600 to 1500 rpm, an increase in the palm biodiesel content in fossil diesel decreased the friction and wear in all conditions (Ref 5). These results were also noted in reviews reported by the same researchers (Ref 6-8), as well as by others (Ref 9). *Calophyllum inophyllum* biodiesel was studied as a lubricity enhancer in wear tests performed by Habibullah et al. (Ref 10). The authors used the four-ball wear test and different diesel–biodiesel blends and loads. The results confirmed that wear decreases with increasing biodiesel content. The effect of a 20% addition of Karanja biodiesel to diesel on the wear of engine components was investigated during 250-h endurance tests in a four-stroke, four-cylinder, 2520-cc diesel engine. Parts such as inlet and exhaust valves, cylinder liners, pistons, piston rings, cranks, and pins were analyzed by weight loss and physical measurements to measure wear. Under these conditions, no severe wear was observed when compared to fossil diesel (Ref 11). Using a simulator test rig prototype, a similar investigation was performed by Reddy et al. (Ref 12) on the effect of biodiesel blends on the wear of mechanical fuel injection systems. The results showed that biodiesel blends presented lower wear as compared to that of diesel in some fuel injection components. Using a pin-on-disk apparatus, Hamdan et al. (Ref 13)

Arlei Franz Venske, Victor Velho de Castro, Eleani Maria da Costa, and **Carlos Alexandre dos Santos**, Pontifícia Universidade Católica do Rio Grande do Sul – PUCRS, Av. Ipiranga, 6681, Porto Alegre, Rio Grande do Sul 90619-900, Brazil. Contact e-mail: carlos.santos@pucrs.br.

investigated the influence of biodiesels produced from different vegetable oils and animal fats on the tribological conditions in a disk–pin pair made from tool steel and cast iron. Among the biodiesels studied, soybean biodiesel presented the best performance when considering the sliding friction force and lubrication conditions.

Although many studies correlating biodiesel lubricity to wear resistance can be found in the literature, information about the effects of the chemical composition, microstructure, and heat treatment of stainless steel in the presence of biodiesel on its wear resistance is rarely found. Martensitic stainless steels are high performance alloys, well known for their high wear resistance, hardness, and moderate corrosion resistance, mainly in the hardened condition obtained after a quenching and tempering heat treatment (Ref 14). These are iron-based alloys containing 10.5-18 wt.% chromium and 0.6-1.3 wt.% carbon. AISI 440B martensitic stainless steel is typically used in diesel engine components such as specialty nozzles, valve seats, inlet and exhaust valves, and piston rings (Ref 15). In high-pressure fuel injection systems, where components are lubricated directly by fuel, the use of plungers with protective layers of alumina, silicon nitride, silicon carbide, or zirconia, is not new; however, interest in such systems has increased in recent years (Ref 16). Some studies have focused on the identification of candidate materials such as ceramics or ceramic metals to substitute for traditional metallic materials in diesel injection systems. Studies have been conducted to understand and rank materials for heavy-duty diesel fuel injector plungers using different fuels (Ref 17-19) and to investigate the friction and wear of different thin-film coatings in the presence of different fuels (Ref 20). These conditions are critical when misalignment or poor lubrication occurs. However, few studies have investigated tribological interactions between stainless steels and ceramic materials in the presence of biodiesel.

The purpose of this work was to analyze the effect of diesel–biodiesel blends on the wear characteristics of AISI 440B martensitic stainless steel with different microstructures and hardness values. Tests were performed in lubricated conditions using Brazilian commercial diesel B7 (as reference), pure biodiesel B100, and with 20% v/v, 30% v/v, and 50% v/v diesel–biodiesel blends. Tests were also conducted in dry conditions.

2. Experimental Procedures

The chemical composition of the AISI 440B stainless steel was determined by optical emission spectrometry (OES) and is shown in Table 1. The material was received in the form of 120 mm diameter × 500 mm long cylindrical bar, in the annealed condition. The hardness value of the as-received material (annealed) was 251 HBW.

Disks of 20 mm thickness were cut from the bar. The samples were heat-treated in the following conditions: austenitized at 1100 °C for 20 min, quenched in oil at 55 °C, and tempered at 100 and 300 °C for 30 min. Characterization of the annealed and heat-treated conditions was carried out by optical and field-emission gun scanning electron microscopy (FE-SEM), x-ray diffraction (XRD), and hardness testing. Metallographic samples were prepared according to the ASTM E3 Standard (Ref 22) and etched using Marble's reagent. Hardness measurements were taken on substrates using the Rockwell method (Ref 23) and inside and outside the wear tracks by the Vickers method (Ref 24).

A pin-on-disk device based on the ASTM G99 Standard (Ref 25) was used to simulate the sliding contact in the dry and lubricated conditions. Alumina ceramic balls (> 96% Al_2O_3) with 10 mm diameter were used, because there was no metallurgical compatibility between the pin and the disks (Ref 26). The applied load was 14.7 N, sliding speed was 1.8 m/s, and total sliding distance was 4400 m for all the tests. These parameters were chosen to simulate wear in a diesel fuel injector plunger based on previous studies (Ref 17-20). The maximum Hertzian contact pressure, calculated using the elastic modulus and Poisson's ratio for steels (E = 200 GPa and ν = 0.32), was 1.24 GPa, which was higher than the yield strengths of the materials in the annealed conditions, but lower than those in the heat-treated conditions.

Before wear test, the disks were machined to 112-mm-diameter and ground on both faces with #100, #220, #320, #400, #600, and #1200 sandpapers, resulting in a superficial roughness < 0.8 mm. One face of each disk was used for the dry tests and the other for the lubricated tests. Before each test, the disks were cleaned in an ultrasonic bath for 10 min using ethanol and dried using a hand-held hot air device. The wear track width (mm) and volume loss (mm^3) were analyzed for each 400 m sliding distance, in eight locations positioned 45° from each other. All wear track widths were examined using an optical microscope with a 0.01-mm resolution measurement system. Each test was carried out in triplicate in each condition, resulting in 24 wear track width measures for each sliding distance. With the results of wear track width (w) and using Eq 1 as recommended by ASTM G99 (Ref 25), the disk volume loss (V_{disk}) was determined, assuming that the pin wear is insignificant and the wear scar has a semicircular profile generated by the alumina ball counter body, given by:

$$V_{disc} = 2 \cdot \pi \cdot R\left[r^2 \cdot \text{sen}^{-1}\left(\frac{w}{2 \cdot r}\right) - \frac{w}{4}\left(4 \cdot r^2 - w^2\right)^{\frac{1}{2}}\right] \quad (\text{mm}^3) \qquad \text{(Eq 1)}$$

where R and r are the radii of the wear track and the pin.

Using Archard Eq 2 (Ref 27-29), the wear coefficient was calculated by:

$$V_{disc} = k \cdot \frac{L \cdot S}{H} \qquad \text{(Eq 2)}$$

where L is the normal applied load, S is the sliding distance, and H is the disk Brinell hardness.

Table 1 Chemical composition of the AISI 440B steel

Elements (wt.%)						
Fe	**C**	**Si**	**Mn**	**Cr**	**Mo**	**Ni**
79.19	0.71	0.358	0.652	18.710	0.0241	0.247

Table 2 Characteristics of the soybean biodiesel

Property	Values	Limits
Density, kg/m^3 @ 20 °C	878.2	850-900
Cinematic viscosity, mm^2/s @ 40 °C	4.3	3.0-6.0
Water conten, (mg/kg	146.7	200 (max)
Ester content, wt.%	97.2	96.5 (min)
Flash point, °C	172	100 (min)
Free glycerol, wt.%	0.02	0.02 (max)
Total glycerol, wt.%	0.18	0.25 (max)
Monoacylglycerol, wt.%	0.6	0.7 (max)
Diacylglycerol, wt.%	0.1	0.2 (max)
Triacylglycerol, wt.%	0.004	0.2 (max)

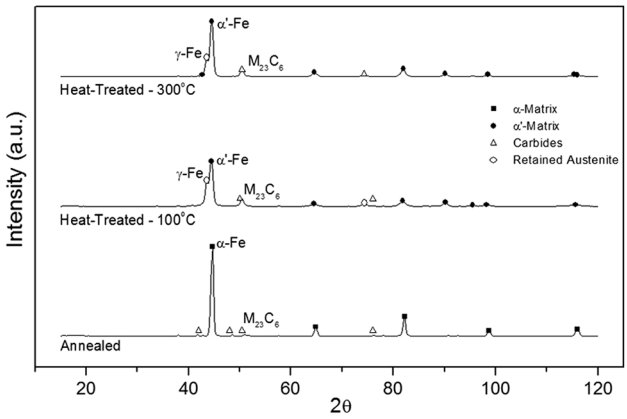

Fig. 3 XRD patterns of the AISI 440B stainless steel: (a) annealed and (b) heat-treated

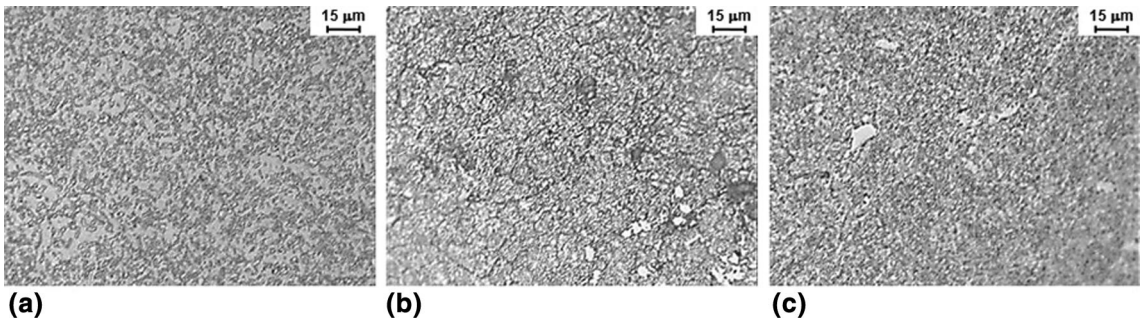

Fig. 1 Optical microstructures of the AISI 440B steel: (a) as received, (b) heat-treated at 100 °C, and (c) heat-treated at 300 °C

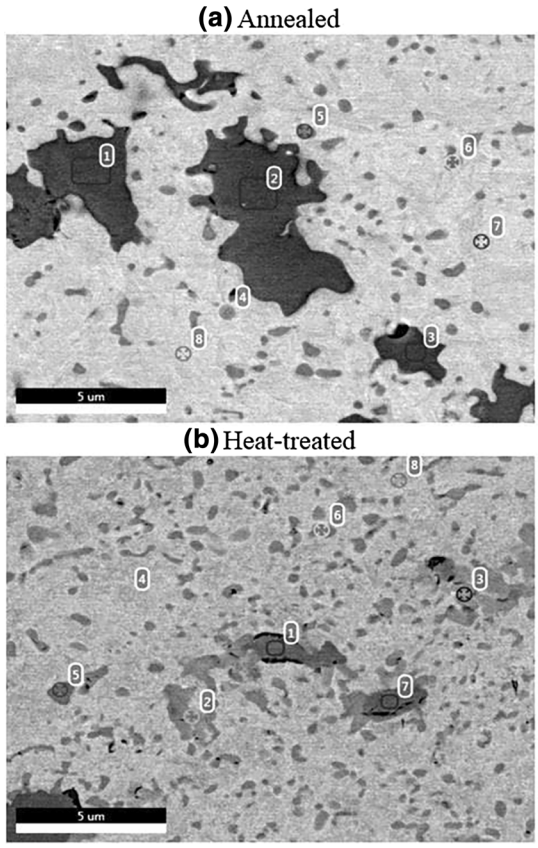

	Element	Weight %
Points 1, 2 and 3 (coarse chromium carbides)	C	7.84
	Cr	64.27
	Mn	1.83
	Fe	26.06
Points 4, 5 and 6 (fine chromium carbides)	C	4.32
	Cr	30.39
	Mn	1.22
	Fe	64.07
Points 7 and 8 (matrix)	Si	0.34
	Cr	18.80
	Mn	0.71
	Fe	80.15
Points 1 and 7 (coarse chromium carbides)	C	4.98
	Cr	41.27
	Mn	1.30
	Fe	52.45
Points 2, 3, 5 and 6 (fine chromium carbides)	C	4.68
	Cr	29.87
	Mn	1.31
	Fe	64.14
Points 4 and 8 (matrix)	Si	0.29
	Cr	19.37
	Mn	0.71
	Fe	79.63

Fig. 2 FE-SEM images of the AISI 440B steel in the BSE mode and EDS analyses of specific areas: (a) annealed and (b) heat-treated

Analyses were performed using Brazilian commercial diesel (fossil diesel with 10 ppm sulfur and 7 vol.% biodiesel—B7), pure biodiesel (B100), diesel–biodiesel blends (B20, B30, and B50–v/v), and in dry conditions. A transesterification process with methanol, sodium hydroxide, and soybean oil was used to obtain the biodiesel. The fatty acid ethyl esters of the pure biodiesel were evaluated in accordance with the EN 14103 Standard (Ref 30), and the main characteristics are shown in Table 2. The biodiesel blend contents were verified by infrared spectrometry (InfraSpec TM VFA-IR, EB) (Ref 31). Wear tests were conducted at room temperature (24 °C ± 2 °C).

3. Results and Discussion

Examination of the as-received AISI 440B stainless steel in the annealed condition showed a microstructure with a ferritic matrix containing dispersed fine and coarse carbides, as shown in Fig. 1(a). In the heat-treated conditions, the microstructures were composed of tempered martensite and carbides for both tempering temperatures, as shown in Fig. 1(b) and (c). Carbides in the heat-treated conditions were somewhat smaller than in the annealed condition, due to heating at the austenitization

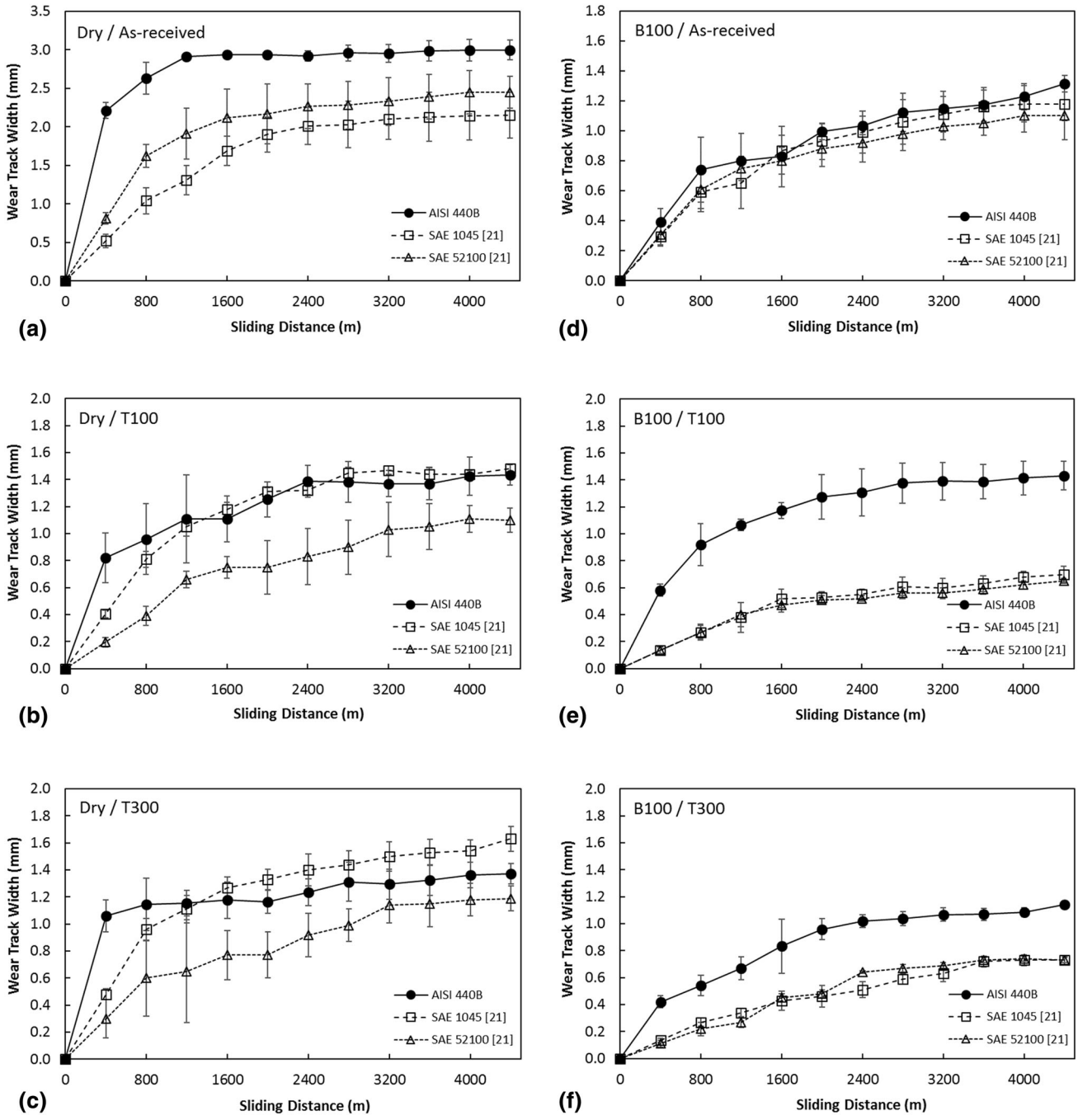

Fig. 4 Wear track widths of AISI 440B steel in the dry condition: (a) as-received (annealed), (b) tempered at 100 °C, (c) tempered at 300 °C; and B100-lubricated condition: (d) as-received (annealed), (e) tempered at 100 °C, (f) tempered at 300 °C, compared to SAE 1045 and SAE 52100 steels (Ref 21)

temperature, which can partially dissolve the carbides (Ref 32, 33). Some retained austenite was present (< 1%), and ferrite was absent.

The AISI 440B stainless steel microstructures were characterized by field-emission gun scanning electron microscopy (FE-SEM) and energy-dispersive x-ray spectroscopy (EDS), in the annealed and heat-treated conditions. Figure 2 shows the microstructures in the backscattered electron mode (BSE) and EDS semiquantitative analyses of the matrix and carbides, as indicated by the points in the images. In both conditions, coarse (dark) and fine (gray) chromium carbides with different chemical compositions were found. The chromium content was higher in the coarse carbides than in the fine carbides.

Figure 3 shows the XRD patterns of the AISI 440B stainless steel in the annealed (as-received) and heat-treated conditions. In the annealed condition, the material consisted of an α-ferritic matrix with chromium carbides ($M_{23}C_6$), while in the heat-treated conditions (tempering at 100 and 300 °C) it was composed of an α'-martensitic matrix, chromium carbides ($M_{23}C_6$), and retained austenite (γ-austenite). These results agree with those reported by Sheng et al. (Ref 35) and Meng et al. (Ref 36), who investigated AISI 440B stainless steel in the untreated and heat-treated conditions.

From the results, it can be concluded that the annealed AISI 440B microstructure had $M_{23}C_6$ chromium carbides embedded in an α-ferritic matrix, while the heat-treated microstructure had the same $M_{23}C_6$ chromium carbides and retained γ-austenite, in a α'-martensitic matrix. In consequence of these microstructures, AISI 440B presented lower hardness value in the annealed condition (20 HRC) than the heat-treated conditions at 100 °C (58 HRC) and 300 °C (56 HRC).

The wear track widths were analyzed as a function of the sliding distance, and Fig. 4 shows the results obtained for the dry and lubricated conditions. The graphs present the average values of triplicate tests and the standard deviations. For the dry condition (Fig. 4a), the AISI 440B stainless steel in the as-annealed condition presented the highest wear track widths, whereas after the heat treatments the values of wear track widths were smaller and similar. This was attributed to the microstructure consisting coarse distributed carbides in a ferritic matrix in the annealed condition, while the heat-treated conditions had tempered martensitic in their matrices. In the presence of B7 to B30 (Fig. 4b-d), the wear behaviors were quite similar for all conditions and higher wear track widths for annealed condition, indicating that the microstructure did not have a significant influence when these diesel–biodiesel blends were used. However, when B50 and pure biodiesel (B100) were used as lubricant (Fig. 4e-f), the 100 °C tempered condition showed the worst behavior, followed by 300 °C tempered and annealed conditions. The observed changes in wear resistance with the use of high biodiesel content seem to be related to the ductility of the matrix. Higher ductility promoted better wear behavior with biodiesel contents superior to 50% v/v. For comparison purposes on the effect of microstructures on wear resistance, experimental data from our previous work for SAE 1045 and SAE 52100 steels have also been discussed (Ref 21). Similar to the AISI 440B steel, the SAE 1045 presented the worst wear behavior in the lubricated conditions with high biodiesel contents. In that case, SAE 1045 had matrix composed of ferrite lamellae pearlite in the annealed microstructure. This confirms that microstructure has effect over the wear resistance as a function of biodiesel content. Furthermore, the size and distribution of hard particles in the matrix also affect wear behavior. When analyzing the effect of hard carbides, it is reasonable suppose that bigger carbides could remove more material by plowing during wear, when considering the same matrix. This was experienced in the samples of AISI 440B which carbides were bigger than in SAE 52100 steel and consequently inferior wear behavior.

According to Fig. 4, for the first 1000 m sliding distance, an initial transient wear regime was noted in the dry condition, mainly for the annealed microstructure, for which the wear rate was higher than in the heat-treated microstructures. After 1600 m, a steady state was achieved. In the presence of biodiesel, the nonlinear state remained until a sliding distance of approximately 3000 m, after which the linear state was predominant. Similar results were observed for SAE 52100

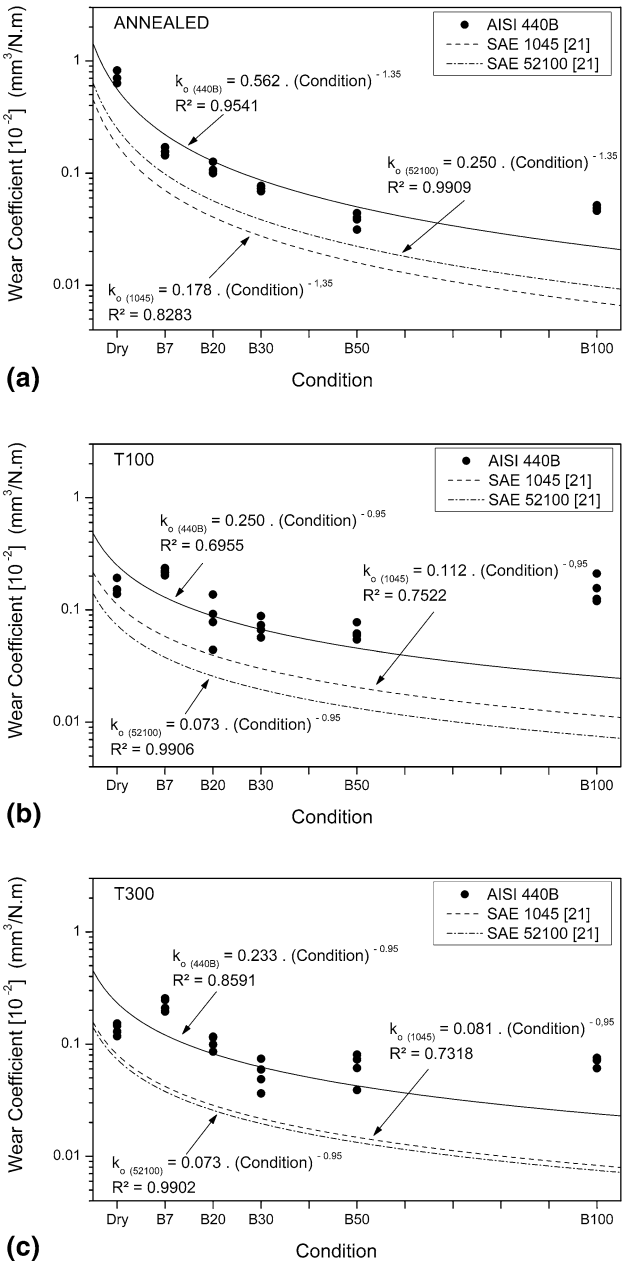

Fig. 5 Wear coefficients of AISI 440B steel in the: (a) annealed, (b) tempered at 100 °C, and (c) tempered at 300 °C, compared to SAE 1045 and SAE 52100 steels (Ref 21)

steel by Habibullah et al. (Ref 10) using *Calophyllum inophyllum* biodiesel and four-ball wear tests at different loads and by Fazal et al. (Ref 5) using palm biodiesel at different speeds.

Figure 5 presents the wear coefficient values after wear testing, which agreed with those presented by Goyal et al. (Ref 37) for a martensitic stainless steel in unlubricated and oil-lubricated conditions. With the wear coefficient as a function of test conditions (Bx—volumetric concentrations of biodiesel added to diesel—v/v), it was possible to build tendency lines based on the equations shown within the graphs. A − 1.35 power law coefficient characterized the experimental variation of the wear coefficient with lubrication for the annealed condition, and a − 0.95 power law existed after the heat treatments. The experimental data obtained by Castro et al. (Ref 21) for SAE 1045 and SAE 52100 steels are also plotted in Fig. 5 (dashed lines) with a view to better discuss the results. The wear coefficient for the annealed AISI 440B varied from 8×10^{-3} to 5×10^{-4} mm^3/Nm for the dry to B100-lubricated conditions. When heat-treated at 100 °C, AISI 440B presented values in the 1.5×10^{-3} to 1.25×10^{-3} mm^3/Nm range, while the heat-treated at 300 °C values ranged from 1.4×10^{-3} to 6×10^{-4} mm^3/Nm. As observed, the wear coefficients for AISI 440B in the lubricated conditions indicated poor wear behavior when compared to the results obtained with SAE 1045 and SAE 52100 steels, for all microstructures, hardness values, and lubrications.

Figure 6 shows the wear track surfaces analyzed by SEM for the annealed and heat-treated AISI 440B steel in the dry condition. Some regions of the wear track are also showed in the highlight areas with high magnification. The annealed AISI 440B presented more areas where material was removed from the surface (large craters). Delamination, scratches, grooves, microcuts, and debris were also observed. After the heat treatments, AISI 440B also demonstrated the presence of small craters, grooves, and microcuts. Analyzing the wear track surfaces and correlating with the wear track widths and wear coefficients, AISI 440B exhibited more severe wear than SAE 52100 and SAE 1045 steels, as investigated previously (Ref 21), despite its higher hardness. This was probably due to the microstructure of AISI 440B, which was composed of coarse hard carbides acting as cutting tools in the ductile ferritic matrix, facilitating the removal of material.

Figure 7 shows details of the AISI 440B wear track and the alumina pin surfaces after testing in the dry condition. The annealed AISI 440B wear surface (Fig. 7a) showed layers that were shaped due to the formation and compaction of wear debris on the contact surfaces. Cracks were also observed in these compacted layers, and this damage was expected to have occurred due to strain hardening of the layer by plastic deformation. In some areas, these layers were smooth and rough in others, resembling "fish scales." As shown in Fig. 7(b), microcracks were present on top of the deformed layers, which could also have promoted debris formation. Transfer of material to the pin occurred in all tests, and the amounts were larger for the annealed samples tested in dry conditions (Fig. 7c). However, the pins were not severely damaged.

Figure 8 presents the sample surfaces when B100 was used for lubricated testing. AISI 440B presented wear damage in all conditions, with deeper craters and grooves. Delamination and microcuts were also observed. After the heat treatments, AISI 440B presented poor wear behavior for both tempering temperatures when compared to annealed condition. This demonstrated that the annealed microstructure presented more wear resistance than the tempered martensitic microstructure in the presence of pure biodiesel.

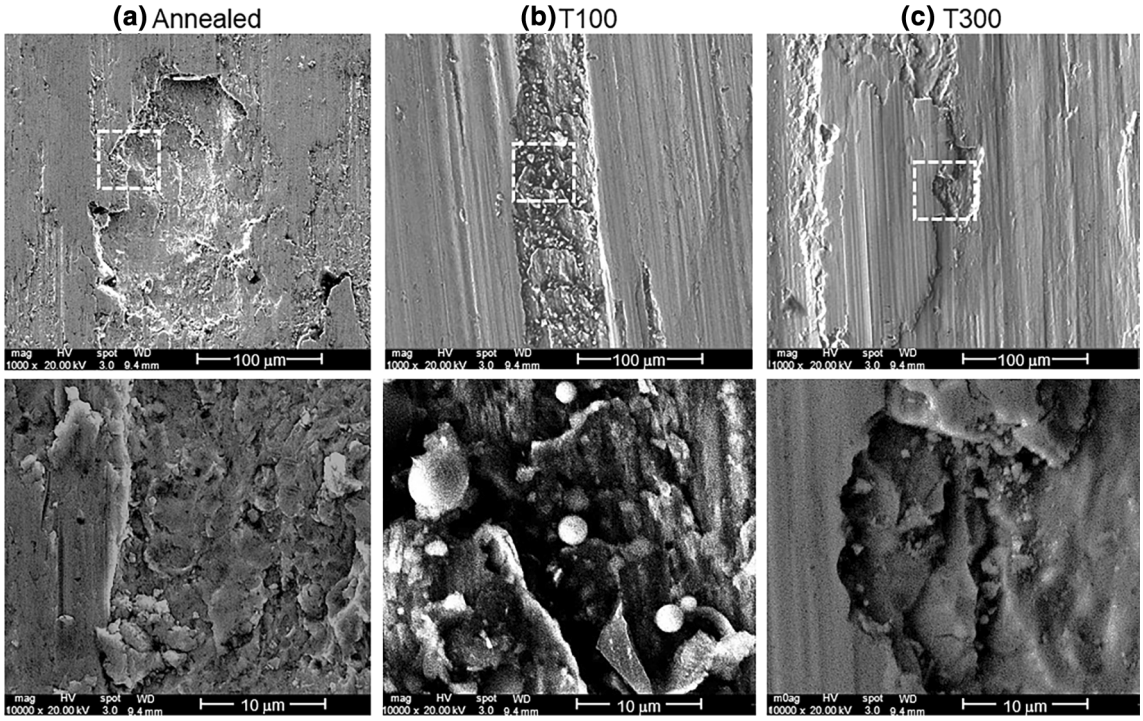

Fig. 6 Wear track surfaces of the AISI 440B steel in the dry condition

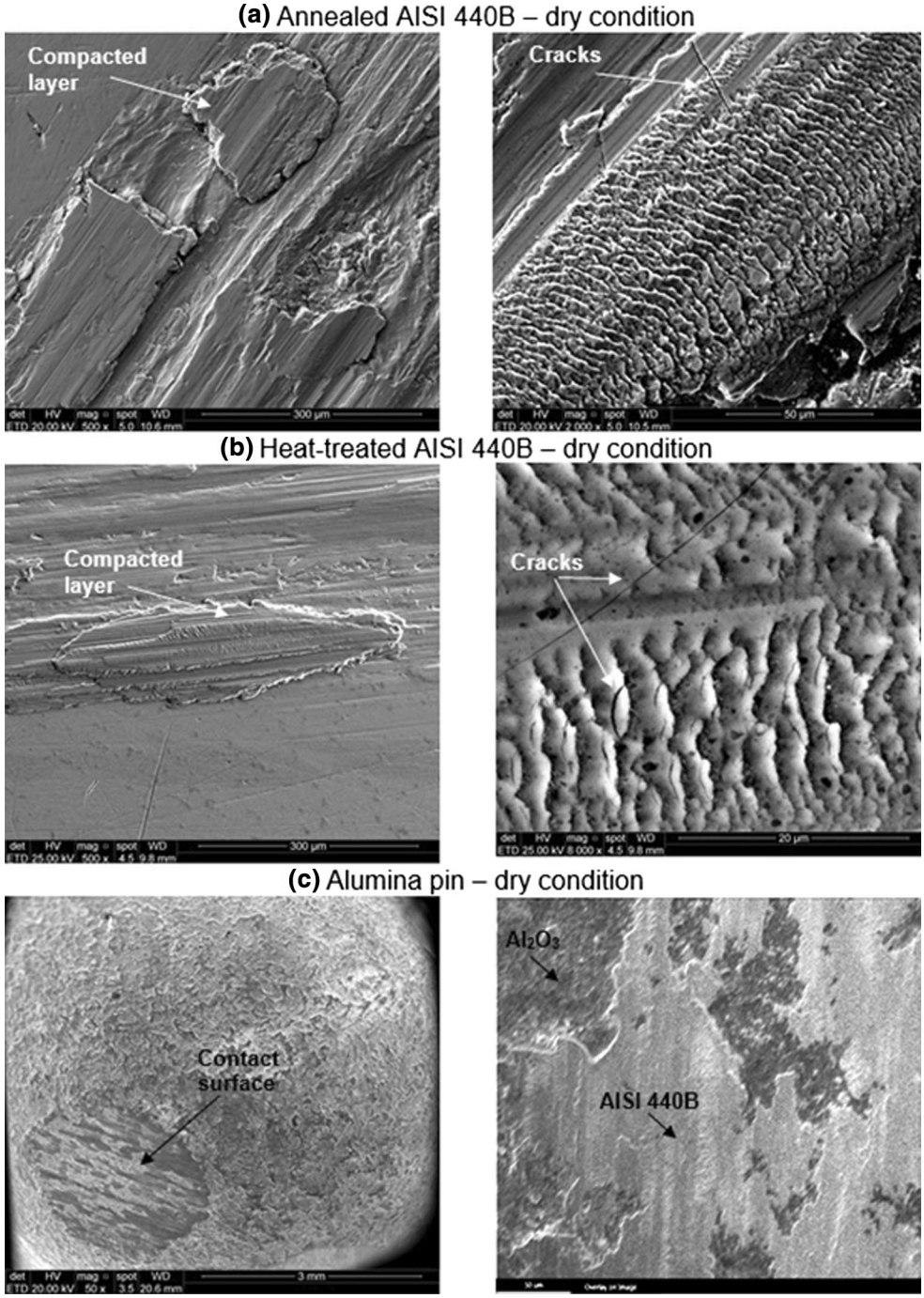

Fig. 7 Details of the wear track surfaces of AISI 440B in dry conditions: (a) annealed, (b) heat-treated, (c) the alumina pin surface

When analyzing AISI 440B in the presence of diesel–biodiesel blends (Fig. 9), the wear decreased with increasing biodiesel content. As expected, the material tempered at 100 °C showed the smallest grooves, delamination, and scratches, followed by the 300 °C tempered and annealed materials. This confirmed that the quenching and tempering heat treatments had a positive influence on wear, where the tempered martensitic microstructure had better wear behavior than the ferrite carbide microstructure (Ref 32-37). With higher biodiesel content (maximum B50 lubrication), wear damage decreased, indicating that lubricity, in terms of friction and wear, decreased in comparison with B7. Detailed analyses of the wear track surfaces showed the presence of carbides (Fig. 10a) and dispersed alumina particles encrusted on the

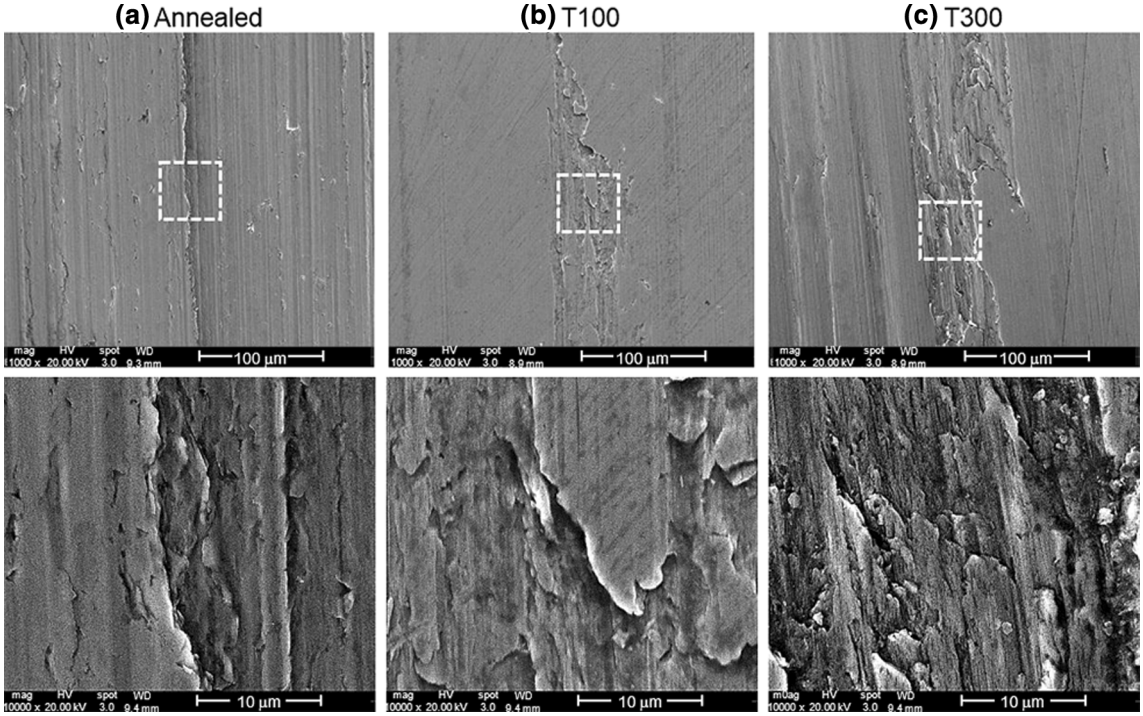

Fig. 8 Wear track surfaces of the AISI 440B steel in the B100-lubricated condition

substrate, mainly for the heat-treated conditions (Fig. 10b). EDS analyses were also performed to confirm the elements in these areas.

Figure 11 shows the variation in Vickers microhardness (inside and outside the wear tracks, for dry and lubricated conditions) and the respective wear coefficients. Comparing the hardness variation inside and outside the wear tracks after dry condition testing, an increase of approximately 68% was observed for the annealed AISI 440B and approximately 13 and 20% increases after the 100 and 300 °C heat treatments, respectively. When lubricated with B100, the hardness increases were approximately 31, 30, and 23% for the annealed and heat-treated at 100 and 300 °C, respectively. By correlating hardness variation with wear behavior, it can be concluded that annealed AISI 440B presented higher strain hardening and a lower wear coefficients in lubricated testing. However, this was not true for the dry condition wear testing. After the heat treatments, the hardness variation decreased and the wear coefficients decreased for B7-B50-lubricated conditions and increased for B100-lubrication.

An analysis of the results from this study suggested experimental equations relating the wear coefficient to the microstructure, hardness variation, and wear condition for the AISI 440B steel, as shown below:

$$\text{Dry} \quad k_o = 0.0711 - (0.00026 * \text{TT}) + (0.008081 * \Delta\text{HV}) + 0.0308R^2 = 0.9310 \quad \text{(Eq 3)}$$

$$\text{Annealed} \quad k_o = 0.2345 - (0.00126 * \Delta\text{HV}) - (0.00168 * \%\text{Biodiesel}) \quad R^2 = 0.9591 \quad \text{(Eq 4)}$$

$$\text{T100} \quad k_o = 0.2524 - (0.00752 * \Delta\text{HV}) + (0.000963 * \%\text{Biodiesel})R^2 = 0.8995 \quad \text{(Eq 5)}$$

$$\text{T300} \quad k_o = 0.2092 - (0.00255 * \Delta\text{HV}) - (0.00103 * \%\text{Biodiesel}) \quad R^2 = 0.9953 \quad \text{(Eq 6)}$$

where TT = 0 (annealed), TT = 100 (heat-treated at 100 °C), TT = 300 (heat-treated at 300 °C), ΔHV = hardness variation inside and outside the wear tracks, and % biodiesel = biodiesel added to diesel—%v/v.

4. Conclusions

The purpose of this research was to analyze the effects of diesel, biodiesel, and their blends, on the wear of AISI 440B martensitic stainless steel with different microstructures and hardness values. Sliding wear testing was performed using a pin-on-disk apparatus. Based on the results, the major new findings concerning the wear of materials were as follows:

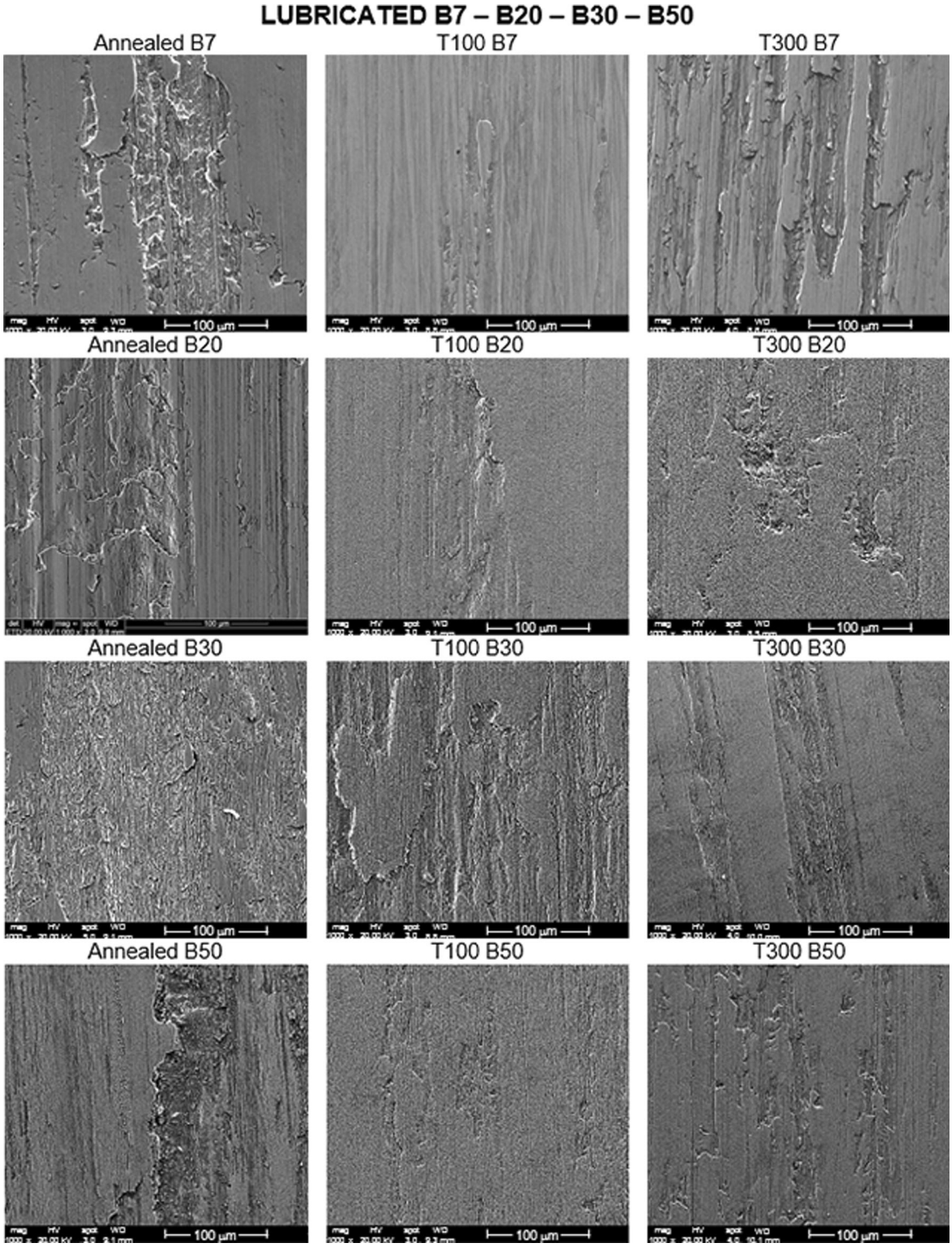

Fig. 9 Wear track surfaces of AISI 440B stainless steel in the B7-B50-lubricated condition range

1. In the dry condition, the annealed AISI 440B stainless steel presented the worst wear behavior due to the ductile microstructure composed of ferrite and carbides. After heat treatments, the wear resistance increased due to the matrix strengthening induced by martensitic transformations. The wear track surfaces indicated severe wear in the dry condition, showing large craters, delamination, grooves and debris.
2. When lubrication was used, it was found that wear resistance increases with increase in biodiesel content for the annealed condition. However, in the heat-treated condition, wear resistance decreased with biodiesel content superior to 50%v/v.
3. The best wear resistance was observed to be related to higher hardness of the microstructure (high strength) in dry sliding condition and lower diesel–biodiesel contents,

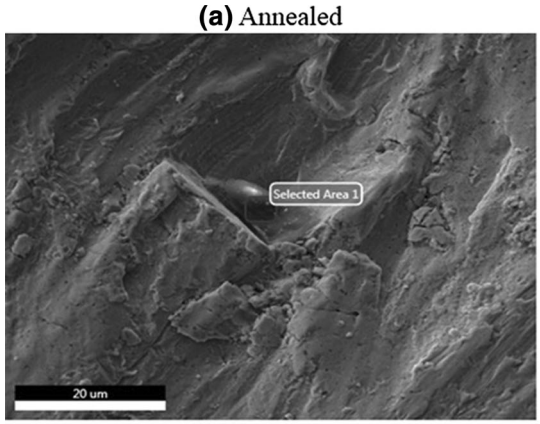

	Element	Weight %
Selected area (complex carbides)	C	64.81
	Fe	22.43
	Cr	4.53
	Mo	0.98
	Si	0.51
	Mn	0.36

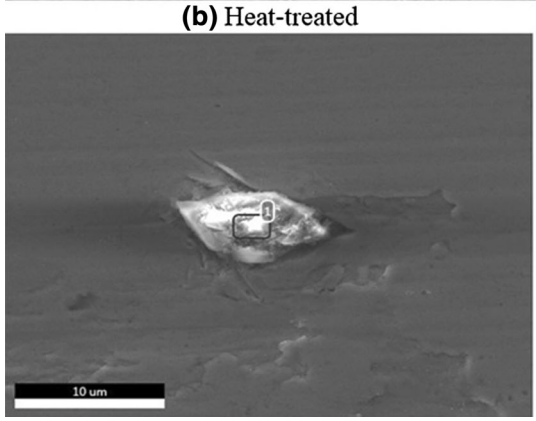

	Element	Weight %
Point 1 (alumina particle)	O	43.38
	Al	56.62

Fig. 10 SEM images of wear track surfaces and EDS analyses of AISI 440B stainless steel: (a) annealed and (b) heat-treated

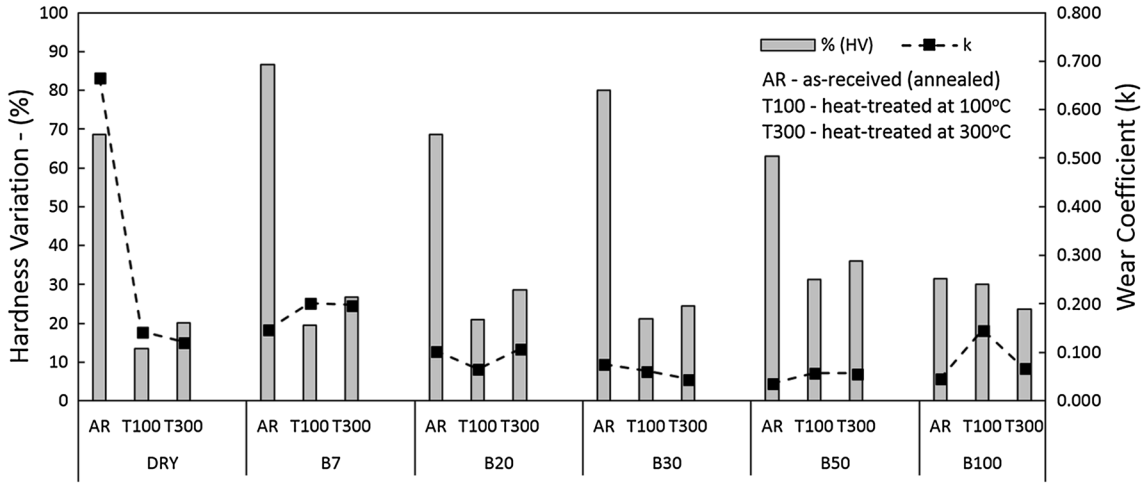

Fig. 11 Hardness variation (inside and outside the wear tracks) and wear coefficients for AISI 440B, compared to SAE 1045 and SAE 52100 steels (Ref 21)

whereas high ductility microstructure increased the tribological properties with higher biodiesel content and pure biodiesel.

4. Experimental equations relating the variation of wear coefficients as a function of lubricated conditions (biodiesel contents) were determined. For the annealed condition, a − 1.35 power law coefficient characterized these behaviors, and for the heat-treated in both tempering conditions a − 0.95 power law coefficient characterized the observed variation.
5. Abrasive wear was observed in all conditions.

Acknowledgments

The authors are grateful to the CNPq (The Brazilian Research Council—Grant Number: 403303/2016-8), FAPERGS (State Foundation for Research of Rio Grande do Sul), CAPES (Coordination for the Improvement of Higher Educational Personnel),

and FINEP (Studies and Projects Financing Agency), for their support.

References

1. ANP – Brazilian National Agency for Petroleum, Oil, Gas and Biofuels. Law no 13263, 3.23.2016
2. F.A. Almeida, M.M. Maru, L.N. Batista, F.J.A. Oliveira, R.R.F.S. Silva, and C.A. Achete, Wear and Friction Behaviour of Si_3N_4 Ceramics Under Diesel and Biodiesel Lubrication, *J. Mater. Res. Technol.*, 2013, **2**(2), p 110–116
3. A. Nicolau, C.V. Lutckmeier, D. Samios, M. Gutterres, and C.M.S. Piatnick, The Relation Between Lubricity and Electrical Properties of Low Sulfur Diesel and Diesel/Biodiesel Blends, *Fuel*, 2014, **117**, p 26–32
4. A.S.M.A. Haseeb, S.Y. Sia, M.A. Fazal, and H.H. Masjuki, Effect of Temperature on Tribological Properties of Palm Biodiesel, *Energy*, 2010, **35**, p 1460, 1464
5. M.A. Fazal, A.S.M.A. Haseeb, and H.H. Masjuki, Investigation of Friction and Wear Characteristics of Palm Biodiesel, *Energy Convers. Manag.*, 2013, **67**, p 251–256
6. M.A. Fazal, A.S.M.A. Haseeb, and H.H. Masjuki, A Critical Review on the Tribological Compatibility of Automotive Materials in Palm Biodiesel, *Energy Convers. Manag.*, 2014, **79**, p 180–186
7. M.H. Mosarof, M.A. Kalam, H.H. Masjuki, A.M. Ashraful, M.M. Rashed, H.K. Imdadul, and I.M. Monirul, Implementation of a Palm Biodiesel Based on Economic Aspects, Performance, Emission, and Wear Characteristics, *Energy Manag.*, 2015, **105**, p 617–629
8. F. Sundus, M.A. Fazal, and H.H. Masjuki, Tribology with Biodiesel: A Study on Enhancing Biodiesel Stability and its Fuel Properties, *Renew. Sustain. Energy Rev.*, 2017, **70**, p 399–412
9. A.K. Agarwal, J.G. Gupta, and A. Dhar, Potential and Challenges for Large-Scale Application of Biodiesel in Automotive Sector, *Prog. Energy Combust. Sci.*, 2017, **61**, p 113–149
10. M. Habibullah, H.H. Masjuki, M.A. Kalam, N.W.M. Zulkifli, B.M. Masum, A. Arslan, and M. Gulzar, Friction and Wear Characteristics of *Calophyllum inophyllum* Biodiesel, *Ind. Crops Prod.*, 2015, **76**, p 188–197
11. A. Dhar and A.K. Agarwal, Effect of Karanja Biodiesel Blend on Engine Wear in a Diesel Engine, *Fuel*, 2014, **134**, p 81–89
12. M.S. Reddy, N. Sharma, and A.K. Agarwal, Effect of Straight Vegetable Oil and Blends and Biodiesel Blends on Wear of Mechanical Fuel Injection Equipment of a Constant Speed Diesel Engine, *Renew. Energy*, 2016, **99**, p 1008–1018
13. S.H. Hamdan, W.W.F. Chong, J.-H. Ng, M.J. Ghazali, and R.J.K. Wood, Influence of Fatty Acid Methyl Ester Composition on Tribological Properties of vegetable Oils and Duck Fat Derived Biodiesel, *Tribol. Int.*, 2017, **113**, p 76–82
14. A.S.M. Handbook, *Properties and Selection: Irons, Steels, and High-Performance Alloys*, Vol 1, ASM International, Russell Township, 1990
15. Villares Metals, Catalog (2011). (http://www.villaresmetals.com.br). (http://www.villaresmetals.nl/english/files/Cat_SS.pdf)
16. J.F. Tovell, Ceramics and the Reciprocating Internal Combustion Engine, *Mater. Des.*, 1984, **5**, p 215–220
17. P.J. Blau, Friction and Wear of a Zr-Based Amorphous Metal Alloy Under Dry and Lubricated Conditions, *Wear*, 2001, **250**, p 431–434
18. J. Qu, J.J. Truhan, and P.J. Blau, Investigation of the Scuffing Characteristics of Candidate Materials for Heavy Duty Diesel Fuel Injectors, *Tribol. Int.*, 2005, **38**, p 381–390
19. J. Qu, J.J. Truhan, P.J. Blau, and H.M. Meyer, III, Scuffing Transition Diagrams for Heavy Duty Diesel Fuel Injector Materials in Ultra Low-Sulfur Fuel-Lubricated Environment, *Wear*, 2005, **259**, p 1031–1040
20. F. Gustavsson, P. Forsberg, and S. Jacobson, Friction and Wear Behavior of Low-Friction Coatings in Conventional and Alternative Fuels, *Tribol. Int.*, 2012, **48**, p 22–28
21. V.V. Castro, L.A.M. Fontoura, J.D. Benfica, M. Seferin, J.L. Pacheco, and C.A. Santos, Lubricated Sliding Wear of SAE 1045 and SAE 52100 Steel Against Alumina in the Presence of Biodiesel, Diesel and a 50:50 Blend of those Fuels, *Wear*, 2016, **368–369**, p 267–277
22. ASTM E3–11, *Standard Guide for Preparation of Metallographic Specimens*, American Society for Testing and Materials, ASM Society, Russell Township p, 2011, p 8
23. ASTM E 18-03, *Standard Test Methods for Rockwell Hardness and Rockwell Superficial Hardness of Metallic Materials*, American Society for Testing and Materials, ASM Society, Russell Township, 2004, p 22
24. ASTM E384-99, *Standard Test Method for Microindentation Hardness of Materials*, American Society for Testing and Materials, ASM Society, Russell Township, 2000, p 24
25. ASTM G99-04, *Standard Test Method for Wear Testing with a Pin-on-Disk Apparatus*, American Society for Testing and Materials, ASM Society, Russell Township, 2004, p 5
26. M. Hua, X. Wei, and J. Li, Friction and Wear Behavior of SUS 304 Austenitic Stainless Steel Against Al_2O_3 Ceramic Ball Under Relative High Load, *Wear*, 2008, **265**, p 799–810
27. J.F. Archard, Contact and Rubbing of Flat Surfaces, *J. Appl. Phys.*, 1953, **24**, p 981–988
28. J.F. Archard and W. Hirst, The Wear of metals Under Unlubricated Conditions, *Proceed. R. Soc.*, 1956, **236–1206**, p 397–410
29. J.K. Lancaster, Material-Specific Wear Mechanism: Relevance to Wear Modelling, *Wear*, 1990, **141**, p 159–183
30. EN 14103, *Fats and Oil Derivatives—Fatty Acid Methyl Esters (FAME)—Determination of Ester and Linolenic Acid Methyl Esters Contents*, European Standard, European Committee for Standardization, Belgium, 2003, p 18
31. ASTM D 7371-12, *Standard Test Method for Determination of Biodiesel (Fatty Acid Methyl Esters) Content in Diesel Fuel Oil Using Mid Infrared Spectroscopy (FTIRATR- PLS Method)*, American Society for Testing and Materials, ASM Society, Russell Township, 2012, p 10
32. K.H. Lo, F.T. Cheng, and H.C. Man, Laser Transformation Hardening of AISI, 440C Martensitic Stainless Steel for Higher Cavitation Erosion Resistance, *Surf. Coat. Technol.*, 2003, **173**(1), p 96–104
33. E. Huttunen-Saarivista, L. Kilpi, T.J. Hakala, L. Carpen, and H. Ronkainen, Tribocorrosion Study of Martensitic and Austenitic Stainless Steels in 0.01 M NaCl Solution, *Tribol. Int.*, 2016, **95**, p 358–371
34. R. Puli and G.D.J. Ram, Microstructures and Properties of Friction Surface Coatings in AISI, 440C Martensitic Stainless Steel, *Surf. Coat. Technol.*, 2012, **207**, p 310–318
35. H.H. Shen, L. Liu, X.Z. Liu, Q. Guo, T.X. Meng, Z.X. Wang, H.J. Yang, and X.P. Liu, Zr/ZrC Modified Layer Formed on AISI, 440B Stainless Steel by Plasma Zr-Alloying, *Appl. Surf. Sci.*, 2016, **388**, p 126–132
36. T.X. Meng, Q. Guo, W. Xi, W.Q. Ding, X.Z. Liu, N.M. Lin, S.W. Yu, and X.P. Liu, Effect of Surface Etching on the Oxidation Behavior of Plasma Chromizing-Treated AISI, 440B Stainless Steel, *Appl. Surf. Sci.*, 2018, **433**, p 855–861
37. V. Goyal, S.K. Sharma, and B.V.M. Kumar, Effect of Lubrication on Tribological Behaviour of Martensitic Stainless Steel, *Mater. Today: Proceed.*, 2015, **2**(4-5), p 1082–1091